Soft Matter

PAPER

Published on 08 July 2026

Cite this: *Soft Matter*, 2026, **22**, 4800

The importance of sub-nanosecond relaxations on the ballistic impact resistance of cross-linked thermoset network polymers

Christopher L. Soles, *[a] Kanae Ito,[b] Christian Yoon,[c] Adam B. Burns,[a] Katherine M. Evans,[a] Polette J. Centellas,[a] Adam J. Biacchi,[d] Angela R. Hight Walker,[e] Madhusudan Tyagi,[f] Timothy W. Sirk,[g] Joseph M. Dennis,[g] Kevin A. Masser,[g] Joseph L. Lenhart,[g] Kohei Sasaki,[h] Naoyuki Shoji,[h] Takefumi Yamashita,[ij] Hiroshi Akiba,[k] Yoshinori Ohmasa[k] and Osamu Yamamuro[kl]

This manuscript explores the importance of the collective, many atom relaxations that occur in cross-linked glassy polymer networks on the picosecond to nanosecond time scale on the mechanical toughness of these materials under ballistic rates of deformation. The relevant strain rates that are generated during ballistic impact events can readily exceed 10^6 s^{-1} and our premise is that a strong population of relaxation mechanisms faster than the time scale of deformation are important to dissipate energy during impact. Our study focuses on a broad range of cross-linked networks, including several different epoxy resins with variations in their network chemistries and a norbornyl-based network cross-linked by ring opening methathesis polymerization. The glass transition temperatures across this series of networks varies by nearly 200 K, leading to wide variations in the materials ballistic impact resistance. The ballistic impact resistance of these cross-linked networks in the glassy state are characterized by variable temperature ballistic gas gun tests while the temperature dependent relaxation dynamics in the nanosecond to picosecond regime are quantified by inelastic and quasielastic neutron scattering. We observe striking similarities between temperature dependent ductile-to-brittle transitions in these materials from the ballistic impact tests and the thermal activation of the collective relaxations on a timescale of 1 to 2 ps, suggesting that activating these relaxations are important for ballistic resistance. Furthermore, we explore the ratio of the collective relaxations on the picosecond time scale to all of the sub-picosecond collective vibrations, that includes the Boson Peak, seems to indicate that the ability of a glass to parlay soft, collective many-atom vibrations into collective relaxations is a key indicator of ballistic impact resistance. The nature and origins of these dynamics correlations are discussed in detail, including some of their potential limitations.

Received 8th April 2026,
Accepted 25th June 2026

DOI: 10.1039/d6sm00313c

rsc.li/soft-matter-journal

[a] *National Institute of Standards and Technology (NIST) Materials Science and Engineering Division, 100 Bureau Drive, Gaithersburg, MD 20899, USA. E-mail: csoles@nist.gov*
[b] *General Support Division, SPring-8, Japan Synchrotron Radiation Research Institute (JASRI), 1-1-1 Kouto, Sayo, Hyogo 679-5198, Japan*
[c] *Poolesville High School, Science, Math, Computer Science House, 17501 West Willard Road, Poolesville, MD 20837, USA*
[d] *NIST Nanoscale Device Characterization Division, 100 Bureau Drive, Gaithersburg, MD 20899, USA*
[e] *NIST Quantum Measurement Division, 100 Bureau Drive, Gaithersburg, MD 20899, USA*
[f] *NIST Center for Neutron Research, 100 Bureau Drive, Gaithersburg, MD 20899, USA*
[g] *Polymers Branch, U.S. DEVCOM Army Research Laboratory, Aberdeen Proving Ground, Maryland 21005, USA*
[h] *NIPPON STEEL Chemical & Material Co. Ltd, 1-13-1 Nihonbashi, Chuo-ku, Tokyo, 103-0027, Japan*
[i] *Department of Physical Chemistry, School of Pharmacy and Pharmaceutical Sciences, Hoshi University, 2-4-41 Ebara, Shinagawa-ku, Tokyo 142-8501, Japan*
[j] *Laboratories for Systems Biology and Medicine, Research Center for Advanced Science and Technology, The University of Tokyo, 4-6-1 Komaba, Meguro-ku, Tokyo, 153-8904, Japan*
[k] *Institute for Solid State Physics (ISSP), University of Tokyo, Kashiwa, Chiba, 277-8581, Japan*
[l] *Solid State Chemistry Laboratory RIKEN Pioneering Research Institute, Box W-G30, 2-1 Hirosawa, Wako, Saitama 351-0198, Japan*

Introduction

Thermoset or cross-linked polymer networks are widely used as the binders in polymer matrix composites. The reactive monomers generally have low viscosity and can be readily infused into a network of stiff, high-strength fibers or inorganic filler particles and then thermally cross-linked around the fillers to create a polymer matrix composite. One of the most widely utilized strategies in polymer matrix composites is to combine thermosetting epoxy resins with high strength carbon fibers to realize high-strength, light-weight systems. Carbon fiber-epoxy composites are increasingly used in a range of commercial and military applications related to buildings and construction, transportation and vehicles, aerospace, athletics, and protective equipment. In many of these applications, it is desirable to have the composite maintain its performance over a wide range of temperatures, extending from the deeply sub-ambient to temperatures that can exceed 200 °C. One of the most important properties for a structural composite material is mechanical toughness. Retaining toughness across such a broad temperature range is a challenge for most epoxy resins. Lower T_g epoxy formulations that offer toughness under ambient conditions often become embrittled at sub-ambient temperatures. High T_g epoxy formulations that offer strength and thermal stability unfortunately tend to be brittle and lead to poor fracture resistance of the resulting composite. This lack of toughness becomes especially problematic at the ultra-high rates of deformation that are associated with ballistic impacts.

Over the past decade, several studies have focused on quantifying the level of energy dissipation in a wide range of cross-linked thermoset network polymers under ballistic impact conditions across an extreme range of temperatures.[1–8] These studies have mostly focused on the neat resin, without fibers or fillers, to develop a molecular understanding of what gives rise to energy dissipation, and therefore toughness, at the rates of deformation that are relevant for ballistics, *i.e.*, strain rates in excess of 10^6 s^{-1}. The ability of an epoxy formulation to dissipate energy at these ballistic rates is operationally defined by making multiple panels of the same material and shooting identical projectiles, each at a fresh panel, with increasing incident velocities until the point at which 50% of the panels are penetrated by the projectile. This critical velocity is defined as V_{50}. By knowing the mass of the projectile and V_{50}, one can define KE_{50} as the ballistic impact resistance, the kinetic energy of a projectile needed to penetrate 50% of the panels. KE_{50} is an operationally defined performance metric relevant to ballistic impact resistance, but not a true measurement energy dissipation or material toughness.

This manuscript focuses on the mechanisms that dissipate energy and contribute to the toughness of cross-linked thermoset glasses. For decades it has been appreciated that relaxations in the glassy state are important for mechanical toughness in polymers, *i.e.*, that having an active mechanical relaxation is important for energy dissipation.[9–12] Seminal works by Boyce, using a variety of impact testing configurations that push the deformation rates into the sub-ballistic regime (strain rates nominally up 10^4 s^{-1}) have shown that when the rate of mechanical deformation exceeds the characteristic relaxation time of the sub-T_g relaxation (often called the β relaxation) in the polymer glass, the stiffness and yield strength of the material goes up.[13–15] The interpretation is that when you deactivate the energy dissipation mechanism by not giving the material enough time to respond to the impulse, the glass becomes stiffer but also more brittle. However, there is still a disparity between the time and length scales of the molecular mechanisms that dissipate energy under ballistic rates of deformation, in excess of 10^6 s^{-1}, and the characterization techniques that are used to quantify the relevant relaxations. As a general statement, we still cannot predict the ballistic response of glassy polymers from our current knowledge of polymer relaxations.

We recently initiated an effort to close this gap by exploring correlations between the level of anharmonicity in the atomic mean square displacement, $\langle u^2 \rangle_{excess}$, of polymer glasses as quantified by incoherent neutron scattering and their corresponding toughness.[16] Across a homologous series of polycarbonates (PCs) with systematic variations in their toughness, we observed a strong correlation between $\langle u^2 \rangle_{excess}$ and the quasi-static impact strength. Our assertion was that the large ''excess'' mean-square atomic displacements measured in the tough PCs, reflecting collective molecular relaxations on the sub-ns timescale, are the signature of incipient dissipative relaxations. However, these measurements based on a Debye–Waller analysis of the elastic incoherent neutron scattering intensities did not precisely resolve the timescale of the motions, beyond identifying that they were faster than the approximately 1 ns resolution of the spectrometer. In a second manuscript,[17] we quantified the full energy spectra of the scattered neutrons to better define the dynamical processes and relevant time scales that underpin these observed motions in the quiescent glass. These measurements were performed as a function of temperature (T) from deep in the glassy state to well above room T, traversing the brittle-to-ductile transition (BDT) of a tough PC glass. We observed that the onset of nonlinear anharmonic fluctuations as quantified by $\langle u^2 \rangle_{excess}$ (relative to the low T harmonic vibrations that contribute to an increase of $\langle u^2 \rangle$ that evolves linearly with T) coincides with the emergence of a relaxation process with a characteristic time scale of $\tau \approx 3$ ps that starts to dominate the QENS spectra. This is the typical order of magnitude for the fast beta relaxation time that is seen in neutron scattering.[19,20] The onset of this relaxation coincided with the BDT temperature, suggesting that many-atom, collective relaxations underpin macroscopic toughness. In our previous publication, we estimated that the size of these collective motions was on the order of (5 to 20) nm^3, and noted these dimensions were on par with the activation volume of yielding in typical polymer glasses.[17]

With respect to our goal to develop a general understanding of the ballistic impact resistance in polymer glasses, the study here contains two important extensions from our previous publications on correlating quasielastic neutron scattering with mechanical properties. First, our previous studies focused primarily on a homologous series of PCs with different modifications, either through copolymerization schemes or small

molecule additives; we have yet to establish the validity of these correlations across a broader range of polymer glasses. This was partially addressed in a third paper where we established the importance of the amplitude of the ps relaxations on the toughness in a series of polynorbornylene copolymers with systematic variations in the level of intermolecular hydrogen bonding; more hydrogen bonding decreased the molecular fluctuations and decreased the quasistatic fracture toughness.[21] The second advance presented here is that all of our correlations with anharmonic collective relaxations and toughness have been under quasi-static mechanical testing conditions (notched Izod impact strength, three point bend K_{IC} tests); we have not extended these studies to true ballistic impact conditions.

In the current manuscript we make the critical leap to address these shortcomings by extending our studies to a broad series of cross-linked network systems that have been studied extensively in terms of the temperature dependence of their KE_{50} ballistic response. This includes a series of diglycidyl ether of bisphenol A (DGEBA) epoxies cured with flexible polyetheramine cross-linkers with variations their molecular mass (the classic Jeffamine series D230, D400, and D2000 where n is approximately 2.5, 6.1 and 33, respectively) or the relatively stiff 4,4′-diaminodicyclohexylmethane (PACM) diamine cross-linking agent. We also include in our comparison the well-studied, ring opening metathesis polymerization (ROMP) network polydicyclopentadiene (pDCPD). The chemical structures of these cross-linked networks are shown in Fig. 1 and the synthetic details of how the networks are prepared are documented elsewhere.[5,6] Several of the relevant materials properties, including T_g, density, molecular mass between cross-links, storage modulus and quasi-static toughness (values previously reported elsewhere[1–3,5,6,18]) are reproduced in Table 1. In the current manuscript, we map both inelastic neutron scattering (INS) $\langle u^2 \rangle_{excess}$ measurements and QENS measurements onto the KE_{50} values over a wide range of temperatures to further explore potential connections between fast, sub-ns relaxations and ballistic impact resistance in a broad range of materials.

Table 1 A summary of some of the key materials of the polymer networks studied here. These include the calorimetric glass transition temperature (T_g), room temperature density (ρ_{RT}), average molecular mass between cross-links ($M_{c,a}$), room temperature Young's storage modulus (E'_{RT}) and the room temperature quasistatic fracture toughness (K_{1C} RT). The values and uncertainty of these data have all been published previously[1–3,5,6,18]

Material	T_g (K)	ρ_{RT} (g cm^{-3})	$M_{c,a}$ (g mol^{-1})	E'_{RT} (MPa)	$K_{1C\ RT}$ (MPa m$^{0.5}$)
PACM	437	1.158 ± 0.003	370 ± 20	2470 ± 120	0.69 ± 0.08
pDCPD	415	1.041 ± 0.003	670 ± 40	1702 ± 100	2.19 ± 0.20
D230	369	1.156 ± 0.003	550 ± 30	2750 ± 110	0.76 ± 0.08
D400	328	1.161 ± 0.003	820 ± 80	2500 ± 150	1.48 ± 0.20
D2000	245	1.160 ± 0.003	4013 ± 195	<5	NA

The time and length scales of these fast relaxations are quantified using the INS and QENS facilities at both the NIST Center for Neutron Research (NCNR) and the Japanese Research Reactor 3 (JRR3). As in our previous work, fixed-window elastic scans on the High Flux Backscattering Spectrometer[22] (HFBS) at the NCNR are used to quantify $\langle u^2 \rangle_{excess}$ as a function of T. These INS measurements are complimented by QENS measurements performed on the Angle Focusing Cold Neutron Spectrometer[23,24] (AGNES) at JRR3 to characterize the timescale of these relaxational processes in the ps to ns range. Our hypothesis is that this time window is critical because it represents the first signs of when the fast-optical modes that are readily visible in infrared or Raman spectroscopy, reflecting local bond vibrations, rotations, and fluctuations on the fs time

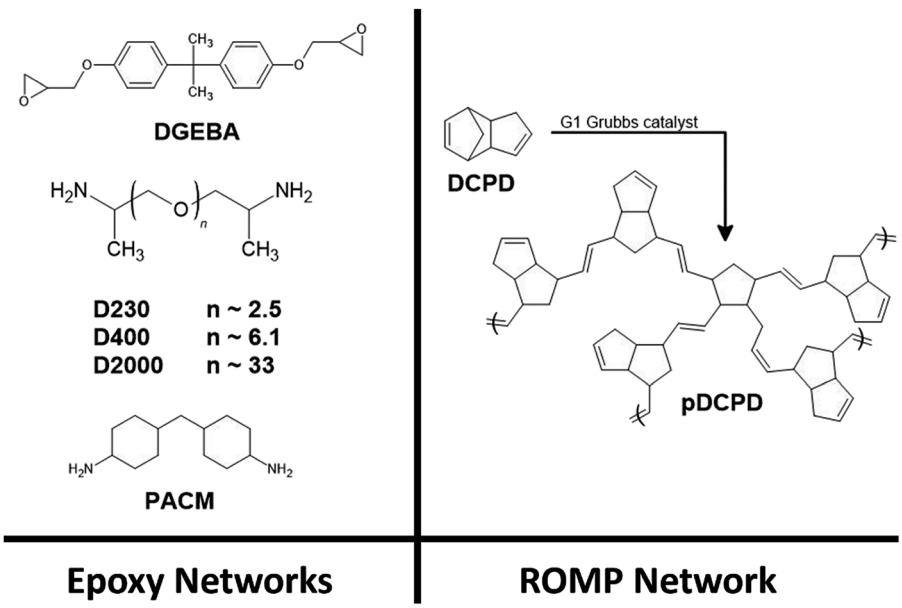

Fig. 1 Schematic chemical structures of the different glassy polymer networks studied here. For the epoxy networks, the DGEBA epoxy monomer is thermally cross-linked with stoichiometric amounts of either the flexible D230, D400, D2000 Jeffamine™ diamines or the rigid PACM diamine. For the ROMP network, the DCPD monomer is cross-linked into a pDCPD network using a first generation (G1) Grubbs catalyst.

scale, start to dynamically couple and give rise to collective motions across 100 s to 1000 s of atoms. The key assertion of our work is that with time scales in the ps to ns range, these motions are sufficiently fast to be active during a ballistic impact event that is characterized by μs time scales and should therefore still be able to dissipate energy.

Experimental†

The epoxy formulations were prepared as mixtures of the desired substituents with a molar ratio of amines to epoxies of 1 to 2, respectively. In general, the reactants were weighed out into a disposable beaker and hand-mixed at room temperature for 5 min until a homogenous mixture was obtained. This mixture was then sonicated for 15 min to remove trapped gases and bubbles in the viscous solution. The solution was then poured into a mold (152 mm × 152 mm × 0.2 mm) with a thickness adequate to minimize multiple neutron scattering events. The general curing procedure was accomplished using a programmable vacuum oven equipped with a nitrogen inlet. The chamber was constantly purged with nitrogen to ensure an inert atmosphere. The cure schedule was: 4 h isothermal at 25 °C, 30 min temperature ramp from 25 °C to 100 °C, 4 h isothermal at 100 °C, 30 min temperature ramp from 100 °C to 200 °C, 6 h isothermal at 200 °C. After the final isothermal step, the oven was turned off and the contents cooled to room temperature over several hours.

Dicyclopentadiene (DCPD) was first melted in an oven at 50 °C, then mixed with 3 mol% of ethylidene norbornene (ENB) to depress the melting point. Then, 5 mmol of triphenylphosphine was added to the DCPD/ENB solution. In a separate container, 2nd generation Grubb's catalyst was dissolved in 1,2-dichloroethane to create a 100 mg mL^{-1} solution. Then, 0.025 mmol of the Grubb's solution was added to the DCPD solution and partially submerged in a sonication bath for 30 s. The sonicated solution was poured into a mold lined with aluminum foil and cured in a vacuum oven (Yamato ADP 21) under flowing N_2 for 2 h at 50 °C, then 1 h at 140 °C. The cured pDCPD film was approximately 200 μm thick.

Measurements of the ballistic performance were carried out as described in previous studies.[6] In short, a gas gun at room temperature (approximately 22 °C), with a relative humidity between 45% and 60%, was used with a 5.56 mm diameter steel ball bearing (Type 302, 0.69 g) to impact the target. The projectile speed was tracked with a Doppler radar (BR-3502, Infinition Inc.), with a velocity resolution of 1 m s^{-1}. The polymer target was oriented such that the projectile impacted the target normal to the sample surface. A witness plate (0.05 mm thick 2024-T3 aluminum foil) was placed 50 mm behind the target. The witness plate was examined for penetration after each shot, with any perforation of the witness plate indicating sample failure. For each epoxy composition investigated, 12 targets were shot. The V_{50} ballistic performance was calculated by taking the arithmetic mean of the three highest non-penetrating and the three lowest penetrating impact velocities on the witness plate. In this way, the V_{50} refers to the velocity required for a penetration probability of 50%. From these velocities, the kinetic energy at a failure probability of 0.5 (KE50) is then calculated. All reported KE50s are normalized by the KE50 of DGEBA/PACM. Further details are provided elsewhere.[6]

The elastic incoherent neutron scattering experiments were performed at the NCNR on the HFBS, located on the NG2 beamline. The polymer films, each approximately 0.2 mm thick, were rolled into the annular sample cans for the instrument and measured under vacuum. The HFBS spectrometer utilizes cold neutrons with a wavelength of 6.271 Å and probes motion over a reciprocal-space range of 0.25 $Å^{-1} < Q < 1.75$ $Å^{-1}$, where Q is the magnitude of the momentum transfer vector, corresponding to real space length scales $2\pi/Q$, or approximately 3.6 Å to 25 Å. The HFBS spectrometer was operated in the "fixed window mode" where the elastic incoherent scattered intensity is measured as a function of Q and T. The 0.8 μeV FWHM energy resolution of HFBS spectrometer means motions slower than approximately 200 MHz appear as static and contribute to the elastic scattering. In this mode, the sample was ramped from approximately 30 K to above well above T_g at a heating rate of 1 K min^{-1}. For elastic incoherent scattering, the Q-dependence of the elastic scattering at each T is approximated with the Debye–Waller factor:

$$I_{\mathrm{inc,elastic}}(Q) \propto \exp\left(-\frac{1}{3}Q^2\langle u^2\rangle\right)$$

Within this model, based on a harmonic oscillator, the slope of $\ln I_{\mathrm{inc,elastic}}(Q)$ *versus* Q^2 is proportional to $\langle u^2\rangle$. It is important to realize that the magnitude of $\langle u^2\rangle$ depends upon the Q range over which the fits are performed. Here we report the linear fits from the low Q region (detectors 1 to 8, Q = 0.25 $Å^{-1}$ to 0.87 $Å^{-1}$) which is consistent with our previous reports of $\langle u^2\rangle$ on polycarbonate materials using the HFBS spectrometer.[16,25,26]

The QENS experiments were performed on the AGNES spectrometer, owned by the ISSP, University of Tokyo, at JRR3 to characterize the quasi-elastic broadening and full inelastic spectra as a function of T (approximately 4 to 7 temperatures per sample, depending on the material) between 100 K and just below the T_g of each material. The AGNES spectrometer was operated in high-resolution mode, significantly sacrificing neutron flux for better energy resolution around the elastic peak. In this mode the elastic resolution is approximately 49 μeV FWHM, accessing a total energy range of approximately (−10 to 1.5) meV. At these settings, the spectrometer is nominally sensitive to motions in the (1 to 100) ps range. Initial attempts to establish a robust Q dependence of the motion proved to be too time consuming, so we opted to average the spectra together across the 0.15 $Å^{-1} < Q < 2.1$ $Å^{-1}$ range of the spectrometer. With the binning of the different Q's, this corresponded to an average value of Q_{ave} = 1.30 $Å^{-1}$ and adequate statistics of the QENS spectra could be obtained in approximately 8 h. The resolution function of the instrument was obtained by cooling either the

† Certain commercial products or company names are identified here to describe our study adequately. Such identification is not intended to imply recommendation or endorsement by the National Institute of Standards and Technology, nor is it intended to imply that the products or names identified are necessarily the best available for the purpose.

D400 or the PACM sample (different materials were run during different beam times) to 4 K where all motions can be considered frozen and collecting a full QENS spectra. The data from both spectrometers were normalized to a vanadium standard and the spectra were fit using the DAVE software package.[27] The uncertainties reported in fit parameters represent one standard deviation in the fitted values.

The QENS spectra from the AGNES spectrometer were fit in the energy range from −0.5 meV and 6 meV, selected to capture the Boson Peak and quasi-elastic broadening while avoiding excessive noise in the negative energy exchange regime. The resolution function for the spectrometer ($S_{res}(Q,E)$) was determined by convoluting one of the 4 K spectra (sufficiently low that all motion is frozen) with a delta function and fitting the strong elastic peak of each of the higher T spectra. An additional flat background (($S_{bkg}(Q,E)$) – line with a slope of zero) was added with its amplitude arbitrarily adjusted to match the scattering intensity at −6 meV. The remaining features of the QENS spectra could be adequately fit by introducing a log normal to capture the Boson Peak, centered in the (1 to 2) meV regime of the spectra, and a narrow Lorentzian to capture the quasi-elastic broadening around the strong elastic peak. The log normal distribution function is defined as:

$$S_{\text{log-normal}}(Q,E) = \frac{1}{\sqrt{2\pi\sigma^2}}\frac{1}{|E|}\exp\left(\frac{-(\ln|E| - \mu)^2}{2\sigma^2}\right)$$

where μ and σ are the center and width of the asymmetric distribution. This empirical model does not invoke any other physics than an asymmetric distribution. The energy of the peak maximum or mode is defined through the relationship $E_{peak} = \exp(\mu - \sigma^2)$. The Lorentzian distribution is defined as:

$$S_{\text{Lorentzian}}(Q,E) = \frac{1}{\pi}\frac{\Gamma}{\Gamma^2 + E^2}$$

where G is the half width half maximum of the peak centered around zero. In both functions, E is the energy axis of the scattering. The resulting final fit is the sum of these four components:

$$S_{fit}(Q,E) = S_{resolution}(Q,E) + S_{bkg}(Q,E) + S_{log\text{-}normal}(Q,E) + S_{Lorentzian}(Q,E).$$

Low-frequency Raman spectroscopy measurements were conducted by 180° backscattering using a microscope equipped with a 100× long working distance objective. A 514.5 nm Ar^+ laser provided the excitation source, and the power of the impinging light was kept at approximately 1.0 mW by employing neutral density filters. The sample was mounted in a liquid nitrogen-cooled microcryostat and spectra were collected beginning at 100 K and then raising the temperature by increments between 10 K and 50 K. The scattered light was directed to a triple-grating (1800 grooves per mm) spectrometer equipped with a charge couple device (CCD) detector, which allowed for the measurement of scattering energies as low as 0.6 meV with a resolution of 0.084 meV. The typical collection time was 300 s.

Low-frequency Raman (LFR) spectra were truncated at 0.62 meV (5 cm^{-1}) to avoid the Rayleigh line (elastic scattering) based on the spectrum of the empty sample holder acquired at room temperature. The spectra cover both the "structural" region ($\lesssim$20 meV) and the beginning of the "fingerprint" or "chemical" region ($\gtrsim$20 meV).[28] The transition between the two is characterized by a precipitous drop in intensity between ∼10 meV to ∼20 meV. The polymer dynamics relevant to this work are reflected in the structural region. The background for each spectrum was constructed using an empirical quadratic fit between ∼30 meV and ∼75 meV. Following background subtraction, the measured intensity $I(E)$ was scaled by the Bose factor $n(E, T) = [\exp(E/kT) - 1]^{-1}$, where E is the Raman shift, k_B is the Boltzmann constant, and T is the absolute temperature of the sample, to facilitate comparisons across the broad temperature range employed herein. The Bose scaled intensity is given by:

$$I_{\text{Bose}}(E) = I(E)/[n(E, T) + 1] = I(E)[1 - \exp(-E/k_BT)].$$

To better understand the origins of the unusually high $\langle u^2\rangle$ values in the PACM network, all-atom molecular dynamics (MD) simulations from a previous study focused on the density of the PACM networks as a function of the degree of cross-linking were used as starting configurations for our analyses here.[29] In this previous study, the networks were modeled with the DREIDING-UT force field.[30] Using AMORPHOUS BUILDER (MAPS, Scienomics), 150 DGEBA and 75 PACM molecules (10 425 atoms total) were initially packed in a cubic box (L_x = L_y = L_z = 60 Å). Curing proceeded under normal pressure and temperature (NPT) conditions (500 K, 1 atm) with CROSS-LINK BUILDER: a cross-link bond was created when the distance between a terminal carbon of DGEBA and a terminal nitrogen of PACM fell below 5.8 Å, consistent with the first O···N radial distribution function (RDF) peak (∼5.5 Å; first shell ∼4.0 Å to 8.0 Å) reported in ref. 24. A Nosé–Hoover thermostat and a Parrinello–Rahman barostat were employed. For each degree of conversion (15%, 45%, 60%, 90%), five independent replicas with mutually distinct cross-link network topologies were provided. After a 2.8 ns heat–cool anneal, 20 ns NPT production runs at 300 K and 1 atm were performed as described previously;[29] the simulated densities semi-quantitatively reproduced the experimental trend. The LAMMPS modeling package was used throughout.

To enable $\langle u^2\rangle$ evaluation at shorter times (t = 50 ps and 100 ps) in the present study, we re-ran 20 ns NPT production simulations at 300 K and 1 atm starting from the cross-linked network configurations reported earlier,[29] using identical settings (force field and thermostat/barostat parameters, timestep, *etc.*) except that the coordinate output frequency was increased to every 1 ps. From these trajectories, we computed all-atom $\langle u^2\rangle$ values at t = 50 ps and t = 100 ps. For each conversion level, we report the replica-averaged means and standard errors (SE) across the five replicas.

Results

A few typical QENS spectra of the D400 material are show in Fig. 2 as a function of T. The data are displayed in terms of the incoherent scattering intensity, $S(Q,E)$, as a function of the

energy exchange E. Incoherent scattering quantifies the Van Hove or self-correlation function of the atoms in the system, with hydrogen having an incoherent scattering cross-section approximately 40 times larger than any of the other atoms in the epoxy. Therefore, QENS is a measure of the hydrogen weighted displacements in the system. As the extremely light hydrogen are attached to the heavier atoms (C, O, N) that are cross-linked into rigid covalent bonds in the polymer network, we take the hydrogen weighted dynamics to be representative of the local chain dynamics in the epoxy network. The E axis of the spectra indicates the energy exchange between the scattered neutron and the dynamic polymer, with positive E reflecting an energy loss in the scattered neutron. In this respect, scattering at $E = 0$ reflects completely elastic scattering (no energy exchange).

For the materials studied here (Fig. 1), a QENS spectra was always obtained at a common base temperature of 100 K. Fig. 2(A) shows the experimental data for D400 at 100 K indicated by small black open circles. Just below the black circles is the elastic resolution function (solid red lines) of the AGNES spectrometer, obtained by cooling the same D400 sample down to 4 K where all the dynamic processes in the materials can reasonably be assumed to be frozen. In Fig. 2(A) at 100 K in the region around $E = (0 \pm 0.5)$ meV there is good overlap between the resolution function and experimental data, indicating most of the scattering is elastic in this regime. At energies higher than 0.5 meV, the experimental scattering becomes stronger than the resolution function, indicating the presence of higher frequency dynamics. It is important to remember that higher energies in QENS mean faster dynamics, or shorter time scales. At 100 K, we are still in the regime where the relaxational modes have not been activated, meaning the dynamics are collective vibrations. The dotted blue lines in Fig. 2 represent the Boson Peak, a collective vibrational mode that is commonly fit with an asymmetric log-normal function. At 100 K, the entire spectra can almost be fit with just a flat background, a Boson Peak, and the elastic resolution function. The overall fits are indicated with the thick solid black line through the experimental data points. Moving through panels (A), (B), (C), and (D) in Fig. 2, the temperature increases systematically from 100 K, 228 K, 268 K, and 288 K, respectively. As the temperature increases, a narrow quasi-elastic mode centered around the elastic line ($E = 0$ meV) emerges. This quasi-elastic broadening is well-described by a Lorentzian function, as shown by the purple dashed line. A Lorentzian in energy space corresponds to a single exponential relaxation in the time domain, occurring at longer times (smaller energies) than the collective vibrations of the Boson Peak. The FWHM of the Lorentzian fits in Fig. 2 are on the order of 0.5 meV, corresponding to a relaxation time of approximately 1.3 ps, whereas the peak values of the higher energy Boson Peaks are approximately 1.7 meV, or a time scale of 0.4 ps. While these are just ballpark values, the exact values for several of the key parameters are plotted below in some of the subsequent figures.

Fig. 3 displays the resulting fits, obtained in an identical manner as explained in Fig. 2, as a function of temperature for all the materials studied here, including D230 (Fig. 3(A)), D400 (Fig. 3(B)), D2000 (Fig. 3(C)), PACM (Fig. 3(D)) and pDCPD (Fig. 3(E)). The breakdown of each fit at each temperature into its individual components, like the data shown in Fig. 2, is

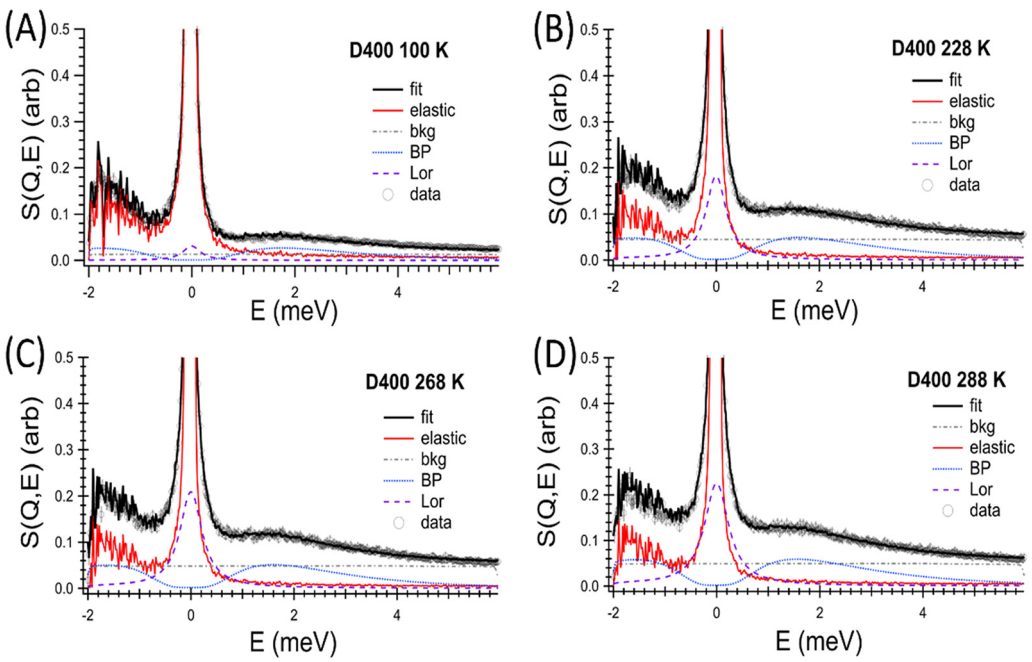

Fig. 2 Examples of the QENS spectra and the corresponding fitting parameters for D400 at the four different temperatures of (A) 100 K, (B) 228 K, (C) 268 K and (D) 288 K. In each panel, the experimental data is indicated by the black open circles. The final fit (solid black line) represents the sum of individual components, including a flat background (bkg, grey dashed dot line), elastic energy resolution of the spectrometer (elastic, red solid line), the log normal function for the Boson Peak (BP, solid blue line) and a Lorentzian for the quasielastic broadening around the elastic resolution (Lor, purple dashed line). Error bars on the experimental data indicate one standard deviation of the scattering intensity $S(Q,E)$ as a function of the scattering energy E.

provided in Fig. S1–S5 of the SI. For each material, the temperatures span from 100 K to just below T_g. As the different resins have different T_gs, the actual temperature ranges are different. PACM has the highest T_g (437 K), so in general these spectra are obtained at higher absolute temperatures; D2000 has the lowest T_g (245 K), so these spectra are obtained at lower absolute temperatures. The spectra here have not been Bose scaled to adjust for trivial temperature variations, so in general, the higher temperature spectra have overall stronger inelastic and quasielastic scattering. Later in the manuscript we will compare the spectra as a function of T–T_g. Regardless, for each material we see the strength of both the inelastic and quasielastic broadening increase with temperature. Note that qualitatively for some of the materials, like D230, D400, and D2000, that the increase of the inelastic intensity reflected in the Boson Peak (log normal function) seems stronger (more dominant) than the increase of the quasielastic broadening (Lorentzian function) around the elastic line. A distinct minimum between the Boson peak and the quasi-elastic broadening or the Lorentzian around the elastic line is visible up to T_g. However, in pDCPD we see extremely strong QES broadening deep in the glassy state, to temperatures well below T_g; a minimum between the quasi-elastic broadening around the elastic line and the Boson peak is not observed. In our previous manuscripts, we argued that such a strong quasi-elastic broadening in the glassy state correlates with mechanical toughness.[16,17,21] This concept will be explored in greater detail below.

In Fig. 4(A) we introduce the experimentally measured ballistic impact resistance, KE_{50}. As stated earlier, KE_{50} is an operationally defined metric of ballistic impact resistance. The measurement is done by shooting a series of identical panels of a material with identical ballistic projectiles where the velocity, or kinetic energy (KE), of the projectile is systematically increased. The velocity at which 50% of the panels catastrophically fail is defined as KE_{50}, or the ballistic impact resistance. This is an operationally defined parameter, not a true measure of toughness, but a standard metric of the materials performance in the ballistic community. In Fig. 4(A) the KE_{50} of the PACM, pDCPD, D230, D400, and D2000 materials are all plotted as a function of T–T_g. These data have been reported elsewhere.[6] All of the KE_{50} data have all been normalized to the value of KE_{50} of PACM at room temperature. The temperature dependence of KE_{50} for the different materials can be generally grouped into three different types of response, which we summarize here. PACM is known to display poor ballistic impact resistance and fail in a brittle manner, never demonstrating toughness. In Fig. 4(A) we see that PACM has the lowest KE_{50} response and its T–T_g dependence is essentially flat; it's always brittle. In the

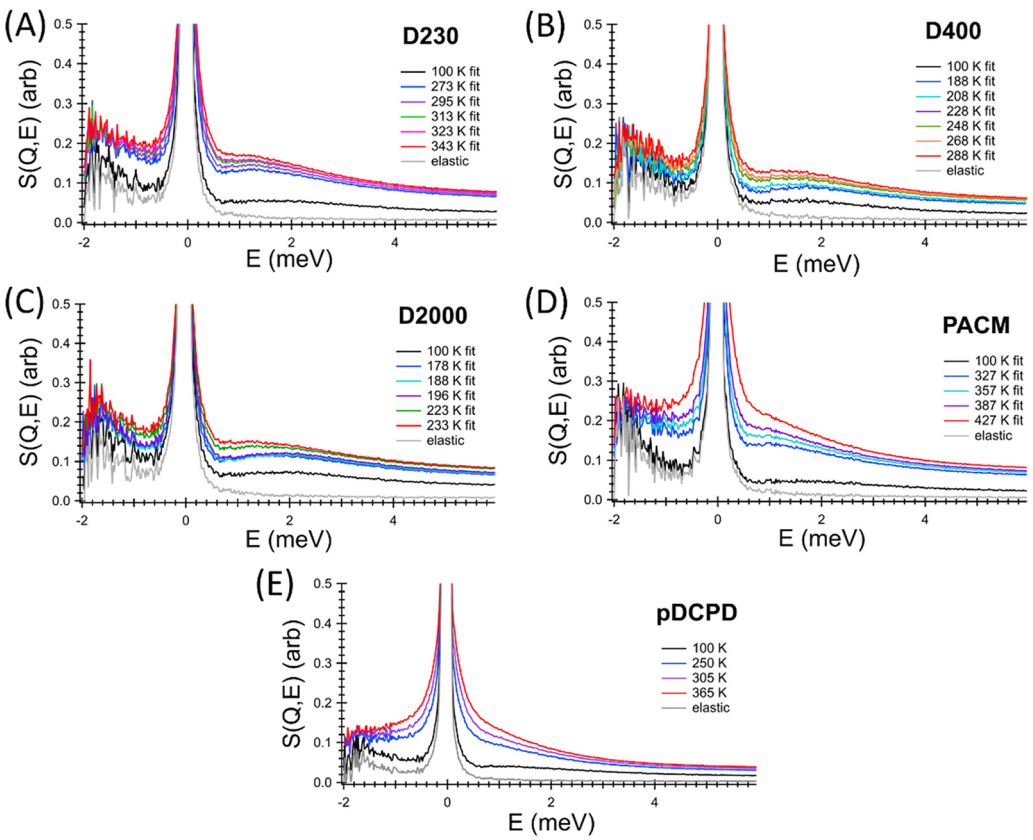

Fig. 3 A summary of all the final QENS fits, as determined in Fig. 2, as a function of temperature for the (A) D230, (B) D400, (C) D2000, (D) PACM and (E) pDCPD networks. In each panel, the legend indicates that as the colors progress from black to red lines, the temperature increases from 100 K to just below the calorimetric T_g of the material. The solid grey line indicates the elastic resolution of the spectrometer. The experimental data symbols for each fit have been omitted for clarity, but the individual fits and experimental data for each curve are provided in the SI.

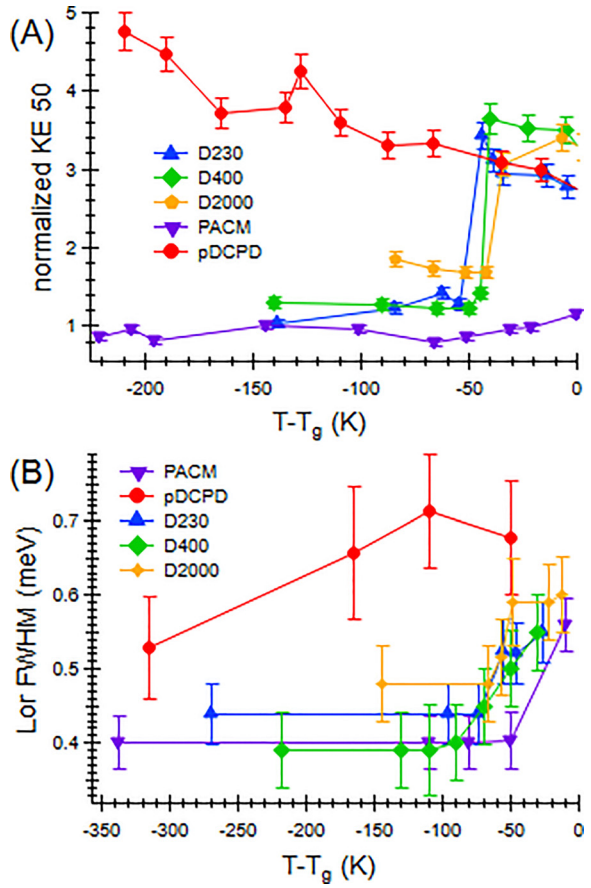

Fig. 4 Panel (A) displays the ballistic impact resistance in terms of the normalized KE 50, as described in the text, as a function of cooling below the glass transition temperature. This representation reveals how the epoxy networks become embrittled upon cooling whereas the ROMP network (pDCPD) maintains tough to deep in the glassy state. Panel (B) shows the corresponding quasielastic broadening of the Lorentzian function across the same temperature regime. This comparison, as discussed in the text, shows a striking similarity between the width of the QES broadening and the ballistic impact resistance, suggesting that the fast relaxations are important for ballistic impact resistance.

D230, D400, and D2000 materials, a clear transition is observed. Just below T_g the materials display excellent ballistic resistance, but when the materials drop approximately 50 K below T_g, a brittle-to-ductile transition occurs. Below the BDT temperature, the KE_{50} of the Jeffamine resins becomes comparable to the brittle PACM. The overlap of these three materials in this T–T_g representation is striking given that the materials have very different absolute T_gs (396 K, 328 K, and 245 K for D230, D400, and D2000, respectively). The T–T_g shifting causes all the curves to overlay, as similarly seen in the Jeffamine series.[6] Finally, there is the curious case of pDCPD. It has a large KE_{50} at T_g, but unlike the other materials it stays ballistically tough upon cooling and slightly increases as the temperature decreases; pDCPD displays superior ballistic impact resistance at temperatures at least 200 K into the glassy state. In terms of absolute temperatures this corresponds to 215 K, strongly in the sub-ambient regime.

In describing the QENS data in Fig. 3, we already commented on how pDCPD displayed strong QES broadening relative to the weaker collective vibrations of the Boson Peak at temperatures deep into the glassy state. In our previous manuscript, we discussed how the relative intensities of the quasi-elastic broadening (Lorentzian) to the collective vibrations of the Boson Peak (log normal) mapped out the ductile-to-brittle transition (DBT) in polycarbonates.[17] At deeply sub-ambient temperatures, where the Boson Peak dominates, the mechanical properties were brittle. However, as the temperature increased and the Lorentzian peak becomes more intense than the Boson Peak, the material transformed into a tough, ductile glass. In this context, the strong quasi-elastic broadening around the elastic line in pDCPD well-below T_g in Fig. 3(E) is consistent with the fact that this material retains excellent ballistic resistance at these same cryogenic temperatures. Turning to the epoxy networks, the intensity of the Boson Peak is either bigger than or on par with the quasi-elastic broadening deep in the glassy state where the KE_{50} values indicate low impact resistance and brittle failure. We explore this concept in greater detail using the temperature dependent fitting parameters for the QES broadening.

To flesh out this comparison further, in Fig. 4(B) we plot the FWHM of the Lorentzian that parameterizes the quasi-elastic broadening around the elastic line of the collective relaxational modes as a function of T–T_g. A broader Lorentzian peak corresponds to faster collective relaxations. In Fig. 4(B) the FWHMs range from approximately (0.4 to 0.7) meV, which in the time domain corresponds to relaxation time constants of (1.6 to 0.9) ps, respectively. In our previous publication on polycarbonates, we used a medium resolution mode on Disc Chopper Spectrometer at NIST where the FWHM of the elastic peak was approximately 0.14 meV, which made it hard to resolve changes in the Lorentzian broadening here when the values were in the (0.4 to 0.7) meV regime. However, using the high-resolution mode of the AGNES spectrometer in Japan, the 0.049 meV FWHM of the elastic peak provides ample resolution to quantify these changes. What became immediately obvious from these higher resolution quasi-elastic measurements is that pDCPD has the broadest Lorentzian component and thus the fastest collective relaxations. Furthermore, these relaxations remain fast and active down to T–T_g values as deep as −300 K. This tracks with the high ballistic impact resistance down to these deeply cryogenic temperatures. By contrast, the fast collective relaxations that are active just below T_g in D230, D400, and D2000 all tend to slow down precipitously when the temperature drops to approximately 50 K below T_g. This directly mirrors the DBT responses in the KE_{50} measurements. As the materials transform from tough and ductile to brittle, the collective relaxations from the quasi-elastic broadening start to slow down.

PACM is a stiff, high T_g epoxy with poor ballistic resistance. In Fig. 4(A) it exhibits brittle failure modes and low KE_{50} values at all temperatures. It is striking that the KE_{50} values of PACM are on par with the KE_{50} values of D230, D400, and D2000 at the lower temperatures where the Jeffamine materials have transitioned to a brittle ballistic response. The FWHM of the quasi-elastic broadening in PACM is generally independent of temperature and on

par with that of D230, D400, and D2000 in their brittle regimes. PACM is always brittle below T_g and has some of the slowest collective relaxations. The only exception to this statement is the single highest temperature datapoint, which corresponds to an absolute temperature of 427 K. This is just 10 K below the actual T_g of 437 K. In general, the quasi-elastic broadening around the elastic line of all polymers, whether brittle or ductile, will always increase significantly at T_g where the elastic modulus of the material softens by an order of magnitude. Given that PACM is a stiff resin, its calorimetric T_g will also be very broad. As reported by Masser and co-workers, the breadth of the calorimetric T_g for PACM is about 14 K, whereas most of the other networks studied here have more narrow T_gs generally in the range of (4 to 6) K.[6] At 427 K it is likely that this last datapoint for PACM is not representative of glassy dynamics, but probably reflects the broad onset of T_g. Polymers above their T_gs will always have strong quasi-elastic broadening but also start to exhibit precipitous drops in their KE_{50} values because of the order of magnitude softening of their elastic modulus. High ballistic impact resistance requires both high stiffness and collective relaxations for energy dissipation.

The similarities in the temperature dependencies of KE_{50} and FWHM of the Lorentzian that quantifies the QES broadening in Fig. 4 is intriguing. In Fig. S16, we use data interpolation methods to establish a strong correlation between the amplitude of the Lorentzian FWHM and the KE_{50} ballistic impact resistance. If we classify $KE_{50} < 2$ as ''weak'' and $KE_{50} > 2$ as ''strong,'' in Fig. S16 we establish that there is an optimized threshold value for the FWHM of 0.514 meV that characterizes 92% of the data points in terms of their transition from weak to strong. This further demonstrates the importance of the fast collective relaxations on the order of 1 ps or longer. In our first publication on this topic we compared a single polycarbonate and looked at the intensity of Lorentzian peak to the intensity of the collective Boson Peak vibrations and related the onset of the quasi-elastic broadening to the quasi-static DBT transition.[17] In another publication on silica nanoparticle composites with densely grafted polymethylacrylate brushes as a function of the brush molecular mass, we reported that a peak in the energy dissipation during a micro-ballistic impact test corresponded to a speeding up of this same quasi-elastic broadening.[31] Here we extend this correlation between the speed of these collective relaxation process and the ballistic impact resistance to a broad range of polymers. We believe that this is an important insight to understanding the ballistic impact of polymer glasses.

In addition to the Lorentzian, we also have the fits to the Boson Peak as a function of temperature for all the materials. The Boson Peak is a common feature in the QENS spectra of amorphous materials deep in the glassy state; it's amplitude and peak position vary from material to material, but it is generally observable in all glassy materials at cryogenic temperatures. The location of the Boson Peak at finite energy distinct from the quasi-elastic broadening in the Lorentzian is indicative of a collection of vibrational modes. The Boson Peak reflects collective, quasi-localized vibrational modes arising from the intrinsic asymmetry of the intermolecular interactions of glassy materials at low temperatures, in combination with the intrinsic granularity of matter on a molecular scale. It is an acoustic-like vibration mode, having many similarities with the transverse acoustic mode phonons familiar from crystalline materials.[32–36] But it occurs in disordered material and is generally believed to represent collective vibrations that span across 100 s to 1000 s of atoms, often related to localized heterogeneities in the elastic modulus.[37–41] Douglas and co-workers have recently suggested that the Boson Peak vibrations consist of one dimensional (1D) collective string-like, or ''stringlet'' vibrations.[42] Regardless of the interpretation, in Fig. 5(A) we plot the peak energy (mode, highest intensity) of the Boson Peak as a function of T–T_g for all of the materials. While there is some experimental scatter in the data, in general the Boson Peaks for each material shift to lower energies as a function of heating in a quasi-linear fashion. A lower energy Boson Peak corresponds to a softer vibration and this type of softening is common for polymer glasses.[42,43] Heating the material softens the collective vibration, which makes sense. We also show in the SI that the area of the Boson Peak generally increases with temperature, indicative of thermal activation. When we compare the energies of the Boson Peak across the different materials, we generally observe that at a given value of T–T_g, the stiffness trend of the Boson Peak is $E_{\text{BP-pDCPD}} < E_{\text{BP-PACM}} < E_{\text{BP-D230}} < E_{\text{BP-D400}} < E_{\text{BP-D2000}}$. At first this trend might seem counter-intuitive because we often associate the stiffness of a network with its T_g, thinking that high T_g networks are stiffer. The T_g trends across the different materials, reported in Table 1, are $T_{\text{g-PACM}} > T_{\text{g-pDCPD}} > T_{\text{g-D230}} > T_{\text{g-D400}} > T_{\text{g-D2000}}$. In this sense, it might seem odd that the higher T_g networks have softer Boson Peak vibrations. However, this is not the case. Soles and coworkers have shown a robust inverse correlation across a wide range of glassy materials (small molecules and polymers) between the stiffness of the Boson Peak vibration and the *ortho*-positronium lifetime τ_3 from positron annihilation lifetime spectroscopy (PALS) measurements that quantifies the size of the local density or packing heterogeneities, sometimes interpreted as free volume.[43] This inverse correlation points to the fact that a more open structure in terms of intermolecular packing leads to a softer Boson Peak. This makes intuitive sense. A more open structure at the intramolecular level leaves more room for the molecules to vibrate and these vibrations are softer due to the reduced nearest neighbor interactions.

Molecular dynamics simulations in PCs have shown that pressure densification in the glassy state leads to a reduction of $\langle u_2 \rangle$, which according to our findings would also reduce toughness.[44] Sokolov and co-workers have also shown that pressure and density will both decrease the amplitude of the Boson Peak and shift the peak to higher frequencies.[45] While we do not have PALS data on these resins, the stiffness of the Boson Peak vibrations nominally tracks the room temperature densities of the materials, which is the macroscopic analog to their packing efficiency. In Table 1 we see that $\rho_{\text{pDCPD}} < \rho_{\text{PACM}} \approx \rho_{\text{D230}} \approx \rho_{\text{D400}} \approx r_{\text{D2000}}$. These trends in the macroscopic densities are generally consistent with our previous PALS results; poor packing efficiencies lead to more open space, lower density, and softer Boson Peaks. It is also well-known

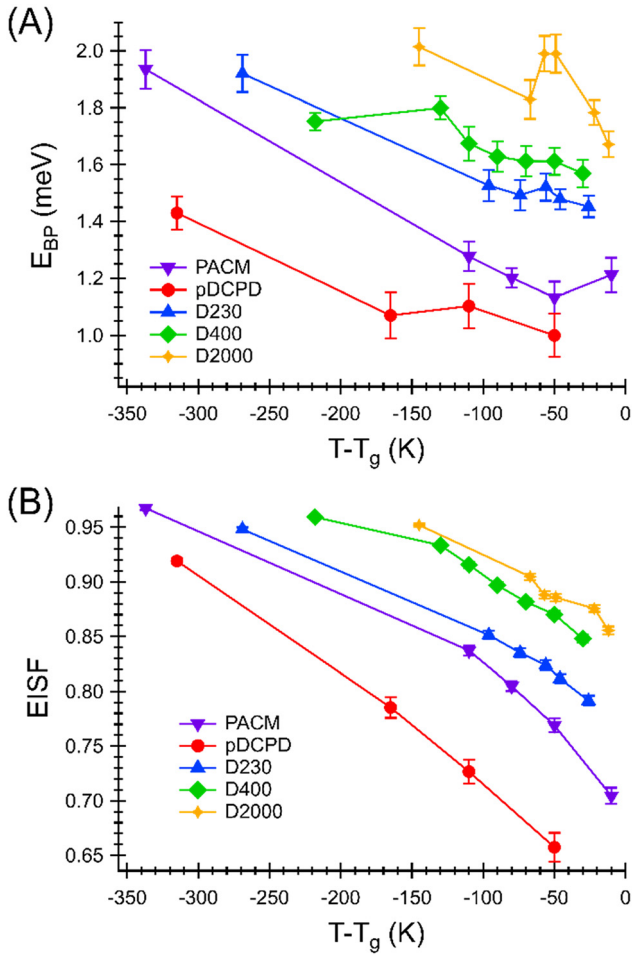

Fig. 5 Panel (A) displays the peak energy of the Boson Peak fit (EBP) as a function cooling below the glass transition for the different network glasses. In general, the collective Boson Peak vibrations stiffen, or shift to higher energies, as the systems are cooled. We also observe that the lower T_g flexible networks, such as D2000 which also has a higher packing density, have stiffer Boson Peak vibrations than the stiffer networks, such as PACM or pDCPD that display poor packing densities. In panel (B) the overall fraction of elastic scattering reflected in the EISF follows a similar temperature dependence as the Boson Peak energies, as discussed in the text.

that high T_g epoxy networks, which usually have stiff epoxies and cross-linking agents, like PACM, exhibit packing frustrations during the final stages of cure. Classic works by Gillham show that the physical density of rigid cross-linking network polymers, including epoxies, decreases during the final (20 to 30)% degree of conversion.[46,47] The steric hinderances become large when trying to reach the final stages of cure with the rigid and non-flexible monomers; this leads to packing frustration and lower density. Gillham and Jean have further shown that these packing frustrations in the final degree of cure lead to an increase in both the size of the packing heterogeneities and the "free volume" fraction from PALS,[48] which infers from our previous results[43] a softening of the Boson Peak. Both MD simulations and physical experiments show that PACM has a non-monotonic trend of density with cross-linking; a peak in the physical density occurs at a cross-link density of 45%, beyond which the structure starts to open up and reduce its density.[29] We have already suggested that materials that can parlay the collective vibrations of the Boson Peak into the relaxations that are seen in the QES broadening are an indicator of mechanical toughness. In this sense, the fact that pDCPD has the softest vibrations seems consistent with this notion. It seems intuitive that it would be easier to parlay soft vibrations into relaxations. However, PACM also has the next softest Boson Peak. The question remains why PACM is not able to parlay its soft vibrations into collective relaxations and toughness? We will return to this question shortly.

The elastic incoherent structure factor (EISF) is another way to parameterize the "stiffness" of a sample with respect to the scattered neutrons. The EISF is defined as the ratio of the integrated intensities of the elastically scattered neutrons over the integrated sums of the elastically scattered plus the inelastically scattered neutrons. According to this definition, an EISF of 1.0 corresponds to completely elastic scattering (no dynamics) as would be the case at absolute zero, whereas an EISF of zero would correspond to no elastic scattering, a situation that might occur in a low viscosity liquid. Here we define the area of the elastic resolution peak over the sum of the areas of the elastic resolution, the Lorentzian, and the log normal Boson Peak. In Fig. 5(B) the EISF is plotted as a function of T–T_g for all the materials. The trends in the EISF mirror the trends in the Boson Peak. At all T–T_g values, pDCPD is the softest material in that it has the least amount of static or elastic scattering. This is consistent with the observation that pDCPD had the softest Boson Peak. By contrast, near T_g the D2000 appears to be the stiffest material with the strongest elastic scattering, consistent with the largest density and the stiffest Boson Peak. Between the extremes of pDCPD and D2000, the trends in the EISF largely follow the same trends found in the density.

Previously we suggested that a salient feature of a tough polymer glass was the ability to parlay the collective vibrations of the Boson Peak into collective relaxations on the ps or longer time scale, that are sufficiently fast enough to dissipate energy during ballistic impact events. The fact that the temperature dependence of the Lorentzian FWHM mirrors the KE_{50} response suggests that this relaxation is relevant to dissipate energy under ballistic impact. To further explore this connection, in Fig. 6(A) we plot the ratio of the integrated intensity of the Lorentzian process (which we define as "good" relaxations with the ballistic impact resistance) to the sum of the Lorentzian (Lor) and the Boson Peak (BP) functions (all dynamics) as a function of T–T_g. This parameter, Lor/(Lor + BP), can be thought of as the relative ratio of the successful relaxations in the system to the number of attempts at executing that relaxation. The results in Fig. 6(A) are largely consistent with the trends reported earlier with the Boson Peak energies and the EISFs. The relative amplitude of the collective relaxations is strongest in pDCPD, consistent with its superior ballistic impact resistance, while it is weakest in D2000. The relative trend between these extremes generally follows the density trend that we have discussed with the Boson Peak energies and the EISFs. It is somewhat surprising and maybe

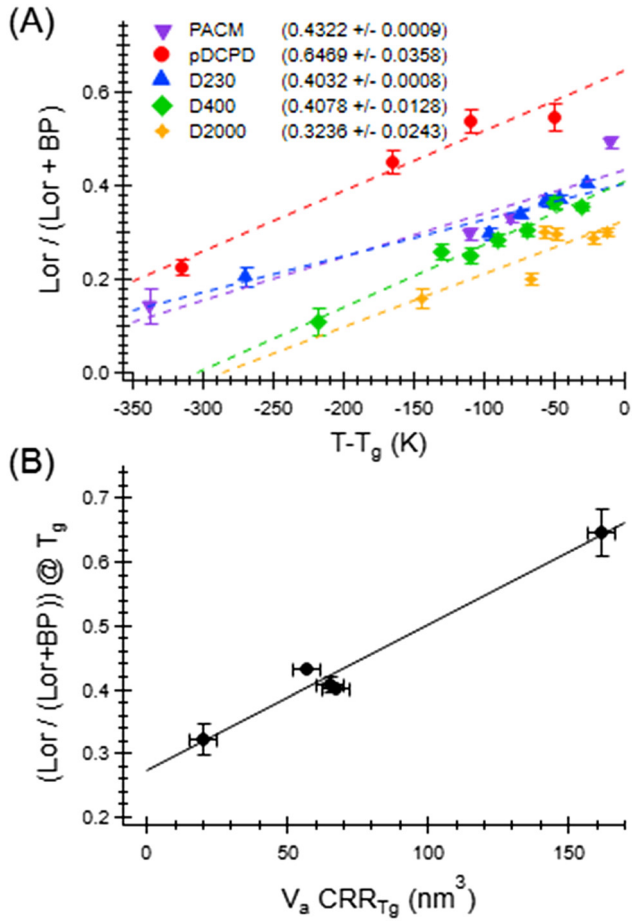

Fig. 6 Panel (A) the ratio of the collective relaxation reflected by the Lorentzian (Lor) over the collective relaxations plus the collective vibrations (Lor + BP) as a function of cooling into the glassy state. In this representation, Lor is the area beneath the Lorentzian peak and BP is the area beneath the Boson Peak. In Panel (A) the thermal dependency of this ration appears linear with the dashed lines indicating linear fits. These linear fits are used to extrapolate the value of this ratio at T_g, which is reported in the legend. In Panel (B) the value of this ratio at T_g is plotted against the volume of the cooperatively rearranging regions determined from the breadth of the calorimetric T_g, as reported previously.

disappointing that this ratio of amplitudes did not map onto the BDT that were seen in the KE_{50} and FWHM data in Fig. 4. The T–T_g dependence is approximately linear. We return to this linear dependence shortly.

In a previous paper, Masser and co-workers used the concepts of Donth[49] and Schick and Donth[50] to estimate the length scale of the cooperatively rearranging regions, CRRs,[51] in the glassy state to estimate the scale of the collective dynamics that lead to a ductile response under ballistic impact. Using this approach, the volume of the CRR at T_g can be estimated from:

$$V_{aCRR} = \frac{k_B T_g^2 \frac{1}{\Delta C_p}}{\delta T \rho}$$

where k_B is Boltzman's constant, T_g is the glass transition temperature, $1/\Delta C_p$ is the reciprocal of the heat capacity step at T_g, δT is the width of the heat capacity step at T_g, and ρ is the density. In their previous study, the authors found a strong proportionality between the breadth of the ductility window below T_g, *i.e.*, (T_g–T_{DBT}), and the volume of the CRRs, $V_{a,CRR}$.[6] This data from their previous publication is reproduced in Fig. S6 of the SI here for convenience. Following a similar approach, linear fits were applied to data in Fig. 6(A) to extrapolate the data and estimate the ratio of Lor/(Lor + BP) at T_g. The extrapolated values of these ratios at T_g with their uncertainties are reported in parenthesis in the caption of Fig. 6(A). Then in Fig. 6(B) we plot the value of Lor/(Lor + BP) at T_g as a function of the previously reported $V_{a,CRR}$. This reveals a surprisingly strong correlation between the relative fraction of the collective relaxation in the glassy state to the size of the cooperatively rearranging regions estimated from the calorimetry data. To the best of our knowledge, this is the first example in which the dynamics from QENS have been implicated in the CRRs. With respect to the ballistic impact resistance, the corresponding connection between the breadth of the ballistic ductility window below T_g and $V_{a,CRR}$ is strong evidence suggesting that the strength of these collective relaxations in the ps time scale as evidence by QENS is important for a ductile response in glassy polymers under ballistic impact.

In our original paper connecting QENS with mechanical toughness, we showed that the BDT occurred when the amplitude of the Lorentzian process surpassed the amplitude of the collective Boson Peak vibrational process.[16] This mapped well onto the onset of anharmonicity in the mean-square displacement measurements in terms of $\langle u^2 \rangle_{excess}$, which we have yet to discuss here. In Fig. 7(A) we plot the $\langle u^2 \rangle$ values from the fixed window scans on the HFBS spectrometer as a function of temperature for these same materials and illustrate how we define the level of anharmonicity in $\langle u^2 \rangle_{excess}$ by subtracting off the contributions from the low temperature harmonic oscillator regime where the temperature dependence is linear. These anharmonic levels of $\langle u^2 \rangle_{excess}$ are plotted as a function of T–T_g in Fig. 7(B). In our previous study on a homologous series of polycarbonates, either plasticized with Arochlor or dynamically enhanced through the copolymerization of cyclohexyl linkages, we observed a strong correlation with $\langle u^2 \rangle_{excess}$ and the quasi-static mechanical toughness. This correlation was observed in a single class of materials, polycarbonate, with systematic variations to their dynamics through either plasticization or copolymerization. Here the correlation appears to break down on the T–T_g comparison across the wide range of epoxy and dicylopentadiene networks studied here. One of the most glaring differences is that PACM has the largest $\langle u^2 \rangle_{excess}$ just below T_g and the worst KE_{50} performance. We will discuss this discrepancy later. In-line with our previous observations, pDCPD has some of the largest $\langle u^2 \rangle_{excess}$ values extending to well below T_g, which would be nominally consistent with its high KE_{50} values. However, we see variations in the magnitudes of $\langle u^2 \rangle_{excess}$ in the T–T_g range of (0 to 100) K regime for D230, D400, and D2000 do not overlap; in Fig. 4(B) the KE_{50} values overlapped beautifully in this T–T_g range. This discrepancy will be discussed below.

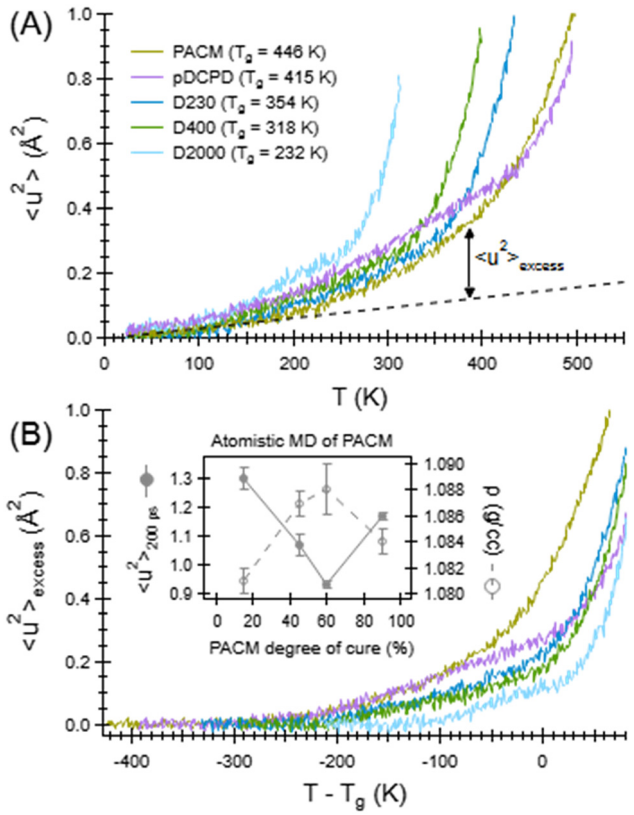

Fig. 7 (A) Displays the mean square displacement $\langle u^2 \rangle$ as a function of temperature for the different cross-linked networks studied here. Panel (A) also shows how $\langle u^2 \rangle_{excess}$ is defined by subtracting the low temperature harmonic vibrations, as described in the text. In panel (B), $\langle u^2 \rangle_{excess}$ is plotted as a function of cooling into the glassy state for comparison with ballistic impact resistance. The inset to panel (B) displays both $\langle u^2 \rangle_{200\,ps}$ and the physical density as a function of the degree of cure PACM from atomistic molecular dynamics simulations, as described in the text.

Discussion

Our previous publications that focused on PCs were the first reports to directly implicate the fast, sub-ns collective relaxations in the glassy state to toughness.[16,17] For decades it has been argued that glassy relaxations engender toughness in polymer glasses,[9–12,52–56] but the role of the higher frequency was largely unexplored. In the late 2000's, Arrese-Igor and co-workers embarked on detailed QENS studies on the dynamics of PCs using both a range of different spectrometers that could access dynamics in the ns to ps time scales, as well as selective deuteration schemes to isolate the dynamics of specific moieties in the PC repeat unit.[57–61] PCs have complicated structures with different local motions that include phenyl ring flips or vibrations, methyl group rotations, carbonate group rotations, and general backbone fluctuations. Their detailed studies were able to account for time and length scales of these different motions to the overall QENS response and the effective $\langle u^2 \rangle$ values. However, a key finding of their studies was that these motions were highly coupled and that "extra" mobility had to be included.[59] This extra, coupled mobility showed up in the window of a (2 to 20) ps regime. In fact, the studies by Arres-Igor were in large part motivated by the fact that PC was such a tough material. In contrast, they also showed that brittle polymer glasses like polystyrene (PS) lacked these extra coupled motions.[62] While they never directly connected these motions to toughness, in our view they were on to a key concept.

In the work presented here, there is a significant diversity in the chemical moieties that make up the different types of network polymers. There are aromatic phenyl rings, aliphatic 4- and 5-member carbon rings, hydroxypropyl ether groups, methyl groups, and primary, secondary, and tertiary amines. It would be nearly impossible to do a tour de force breakdown of the QENS spectra into the different contributions of the different groups in the style of the careful measurements of Arrese-Igor. Furthermore, these are cross-linked networks, and we have no way to precisely determine the cross-linking density. This means that the final chemistry and density as a function of temperature of each material is still vague. We are unable to properly normalize the scattering intensities with the scattering length densities of the elements comprising the network. We have made all the sample thicknesses the same and rely on arbitrary intensities. This is an admitted shortcoming of our study. We have consciously chosen to collect as much QENS data as we can across a broad range of temperatures and then map the QENS response onto the temperature dependent ballistic data. Across such a broad range of materials, this also means we chose to sacrifice collecting statistically significant scattering data to perform a detailed Q dependent analysis of the spectra; we chose to average together over the Q range of the instrument. But even with these limitations, we have observed some interesting correlations with the ballistic impact resistance.

One of the most exciting findings in this paper is the similarity in the temperature dependencies of the FWHM of the Lorentzian broadening around the elastic line and the KE_{50} values. The FWHM of these Lorentzians are the same fast processes or extra anharmonic relaxations that Arrese-Igor focused on in their studies and indirectly inferred that they were important for mechanical properties. We think that it is an important finding here that we directly correlate these fast collective relaxations with mechanical properties, especially at the ballistic rates of deformation. This is an important insight. Activating these processes in terms of the time scale of their motion does affect ballistic impact resistance. Faster relaxations are better able to dissipate ballistic impact energy. This finding is also consistent with our recent micro-ballistic Laser Induced Projectile Impact Testing (LIPIT) studies on the polymer grafted nanoparticles (PGNs) as a function of the graft molecular mass. At intermediate molecular masses for the densely grafted polymer brushes, we observed both an acceleration in these collective relaxations from the Lorentzian broadening and an increase in the ballistic impact resistance using microparticle projectiles traveling at velocities as fast as 1 km s^{-1}.[31] It is salient to point out that later, Fytas and co-workers observed an acceleration in the 12 GHz (~80 ps) motions using Brillioun Light Scattering (BLS) in these same systems at these same intermediate graft molecular masses.[63] These findings paint the picture that these fast collective relaxations are important for ballistic rate impact resistance.

However, as mentioned previously, we also now observe a breakdown of the direct relationship between toughness and $\langle u^2 \rangle_{excess}$ across this broad range of materials. We believe that this breakdown stems from a couple of reasons. First, we turn to the direct comparison between Fig. 7(A and B). This broad set of materials have very different T_gs, spanning over 200 K in absolute temperatures. Dynamics are always thermally activated. Compared on the basis of T–T_g, there is significantly less thermal activation near T_g in the lower T_g D2000 than the higher T_g PACM. These two materials have significantly different T_gs and there will always be more thermal activation at higher T. To address this point, in Fig. S7(A), we present a map in terms of absolute T where the KE_{50} measurements were performed for all of the materials studied here. There is a small window of T_s between (218 to 295) K where we have both KE_{50} and $\langle u^2 \rangle$ data. In Fig. S7(B) we plot the isothermal correlations between KE_{50} and $\langle u^2 \rangle$ for three T_s in this window. The results look promising. When comparing the isothermal trends, there appears to be a strong positive correlation between ballistic impact resistance and $\langle u^2 \rangle$. However, extending this correlation across a larger T range where there are very different states of thermal excitation causes difficulties.

The second difficulty that makes comparisons across the wide range of networks difficult is that the PACM, pDCPD, and the Jeffamine samples are very different in terms of the chemical moieties that make up their structures. As we already discussed, the different materials contain a different mix of aromatic phenyl rings, aliphatic 4- and 5-member carbon rings, hydroxypropyl ether groups, methyl groups, and primary, secondary, and tertiary amines. Many have shown that to properly calculate $\langle u^2 \rangle$, the precise nature and geometry of the motions of the different moieties must be properly accounted for to obtain accurate $\langle u^2 \rangle$ values, which requires access to a very large Q range.[64,65] We have only examined the low Q regime when calculating $\langle u^2 \rangle$ that emphasize longer range motions that are more relative for relaxations, but do not capture these subtle molecular details. It is well known that QENS, especially in the higher energy regimes, is sensitive to the details of the molecular structure. While our discussion has focused on the role of collective relaxations, we have ignored more local contributions like methyl or primary amine rotations. Such rotations are fixed in space, do little to dissipate energy, but can contribute significantly to the QENS signal. To illustrate this point, we return to our discussion to PACM. PACM is a very rigid curing agent which leads to significant steric hindrances during the final stages of the cross-linking process. Yamashita has already shown that PACM is subject to this effect and shows a decrease in density in the final stages of cross-linking.[29] Rawlins and co-workers have likewise shown, in a similar brittle high T_g epoxy, that the fracture toughness decreases in these final stages of cure as the density is decreasing.[66] It is likely that these sterically hindered, high T_g resins never reach 100% conversion, which means there will be a fraction of dangling bonds, such as primary amines, secondary amines, or epoxide groups. As PACM has low physical density, these H containing moieties are probably free to rotate or rattle.

To explore this possibility further, we turn to the previous results of Yamashita as a starting point.[29] From the models they previously published, we calculate the $\langle u^2 \rangle$ values from the trajectories of the MD simulations using both a 50 ps and 100 ps elastic resolution as a function of the degree of conversion in the high T_g PACM network as described in the Methods section. These $\langle u^2 \rangle$ values are reported in the SI with the 100 ps values presented in the inset of Fig. 7(B). These results clearly reveal a non-monotonic trend between the degree of conversion and both the physical density and $\langle u^2 \rangle$. This is entirely consistent with the non-monotonic trends in density with degree of cure reported previously by Gillham and Jean.[46–48] During the final stages of cure, the imposed steric hinderances open the structure up and lead to an artificial enhancement of $\langle u^2 \rangle$ that is not relaxational. These types of localized, non-relaxational motions contribute strongly to QENS and are probably in part why the $\langle u^2 \rangle$ values are so large in PACM.

To illustrate this point further, we performed low frequency Raman (LFR) spectroscopy on these same materials as a function of temperature. Fig. S8–S12 in the SI describe the processing of the LFR data, with a complete set of LFR data for all the materials as a function of T provided in Fig. S13. Here we focus on a comparison of the LFR data for PACM and pDCPD. Unlike QENS, LFR is not extremely sensitive to local motions of groups like dangling primary amines, secondary amines, or hydroxyls. The LFR signal is dominated by groups that have strong polarizability to the 514.5 nm laser that is used in the Raman spectrometer. In these networks, the phenyl groups in the epoxies and pDCPD will dominate the signal. The comparison is striking. In PACM we see that the Boson peak is very distinct at low temperatures and dominates the spectra at temperatures very close to T_g. That quasielastic broadening around the elastic line that was seen in the QENS is completely missing in the LFR. The glassy spectra are largely dominated by either the Boson Peak or non-diffusive motions that do not dissipate energy. By contrast, the quasielastic broadening around the elastic line is very strong in pDCPD. In Fig. S13 the Boson Peak is only visible in the 100 K spectra. At all other temperatures deep in the glassy state the quasielastic broadening dominates. Both QENS and LFR indicate strong glassy relaxations in pDCPD.

In our previous publication, we argued that the amplitude of the Lorentzian process relative to the Boson Peak was important for toughness. We do not plot that data here because we did not see strong correlations with the amplitude of this Lorentzian and the KE_{50} values. But in hindsight this probably reflects the fact that the comparison spans such a large absolute temperature range of several hundreds of K. We did not attempt to Bose scale the QENS spectra (although we did Bose scale the Raman spectra) to normalize trivial temperature variations in the dynamics across these large temperature differences. It is not immediately evident if this would be warranted as we do not precisely know the scattering length density of the different cross-linked networks. Rather, we chose to compare the ratios of amplitudes of the collective Lorentzian relaxations to total dynamics. The Lor/(Lor + BP) across the different materials as a function of T–T_g also warrants further

discussion. By looking at this ratio, we normalize out the large variations in absolute temperature across the different materials. The proportionality between the Lor/(Lor + BP) at T_g and the $V_{a,CRR}$ estimates from Masser and co-workers is exciting. From the results shown in their previous paper[6] indicating a direct proportionality between $V_{a,CRR}$ and the (T–T_{DBT}) ductility window (repeated in the SI), we can conclude that this Lor/(Lor + BP) is important for KE_{50}. It is also interesting to note in Fig. 6(B) that the magnitudes of the $V_{a,\ CRR}$ values reported here nominally range from (25 to 150) nm^3. In our previous publication on polycarbonates, we used the method of Sokolov and co-workers to estimate the volume of material participating in the Boson Peak from the ratio of the frequency of the transverse acoustic mode to the Boson Peak frequency to be on the order of approximately (5 to 20) nm^3. These values are also on par with the activation volume for mechanical yielding estimated from rate and temperature dependent quasistatic toughness measurements.[17] Sokolov has already shown that this volume of the material participating in the Boson Peak is proportional to the activation volume of glass formation in a wide range of materials.[67] It is therefore maybe not surprising that this Lor/(Lor + BP) ratio is related to the $V_{a,CRR}$, a parameter that is directly related to glass formation. All of these length scales are similar. As suggested by Sirk and co-workers, fluctuations at these length scales are probably important for destabilizing void formation and staving off brittle failure.[2,5,7,8,21,68]

As a closing comment, it is worth emphasizing that the dynamics quantified by QENS are spatially averaged across the entire sample. There are now emerging several reports of heterogenous dynamics in cross-linked epoxy networks and how these heterogeneities in turn can affect critical properties.[69–74] Our studies here do not directly address this issue of dynamic heterogeneity. We suspect that our QENS measurements would be affected by dynamic heterogeneities. We have seen evidence of this in our previous works connecting QENS and the density heterogeneities probed by PALS.[21,43,75] The relationship between the level of dynamic heterogeneity and the overall dynamics quantified by QENS is an interesting topic that is worthy of additional research in the context of mechanical properties of polymer glasses.

Conclusions

What these measurements suggest is that glassy polymers that can parlay soft Boson Peaks into collective relaxations on the time scale of longer than 1 ps seem to be a salient characteristic for ballistic impact resistance. We have now shown that this trend is relevant in a series of PC glasses, a series of PGNs with variable graft molecular masses, and now in a broad range of cross-linked network polymers. We have also published a preliminary set of $\langle u^2 \rangle$ results on a series of polydicyclopentadiene materials with systematic variations in the hydrogen bonding capacity that further support this notion,[21] and are in the process of writing up a longer manuscript that expands this comparison to the full QENS spectra. While these insights are exciting, we also warn that there are many caveats that must be considered. The correlations are not always perfect. In this manuscript we saw how comparing dynamics across broad absolute temperature ranges can be a challenge. We also discussed how different measurements, for example QENS *versus* LFR, are selectively sensitive to different types of chemical moieties or motions. These differences must be properly accounted for. But from what we have seen thus far, this seems to be an important aspect to understand the ballistic impact resistance of glassy polymers.

Author contributions

The manuscript was written through contributions of all authors. All authors have given approval to the final version of the manuscript. Christopher Soles, Kevin Masser and Joe Lenhart conceived the study and Christopher Soles was the primary author in writing the manuscript. Samples were prepared by Kevin Masser, Joe Dennis, Polette Centellas, and Katherine Evans. The neutron scattering measurement were performed by Christopher Soles, Madhu Tyagi, Kanae Ito, Hiroshi Akiba, Yoshinori Ohmasa, and Osamu Yamamuro. The neutron scattering data was analyzed by Christian Yoon, Adam Burns, Kanae Ito and Christopher Soles. The low frequency Raman data were collected by Adam Biacchi and Angela Height Walker and analyzed by Adam Burns. The ballistic KE_{50} measurements were performed at the ballistic testing range at the Army Research Laboratory. Tim Sirk, Kohei Sasaki, Naoyuki Shoji and Takefumi Yamashitai performed MD modeling and simulations and assisted with data interpretation and writing. The authors would like to thank Ran Tao, Marcos Reyes-Martinez and Jack Douglas for their careful critiques of the manuscript.

Conflicts of interest

There are no conflicts to declare.

Data availability

The individual QENS spectra reported in this manuscript and their corresponding fits are plotted in SI, Fig. S1–S5. The raw data for these figures have been archived on the NIST Public Data Repository (https://doi.org/10.18434/mds2-4136). This repository also includes the individual DAVE fitting and model files for each of the spectra. The corresponding ''fit dat mod'' files can be load into DAVE for further analysis. These files also contain the numerical fitting parameters. The DAVE software package is freely available through NIST Center for Neutron Research (https://www.ncnr.nist.gov/dave/download.html). The SI also includes plots of width of the ductile response in the glassy state as a function of estimates of the volume of the cooperatively rearranging regions (S6), isothermal comparisons of $\langle u^2 \rangle$ as a function of KE_{50} (S7), a detailed analysis of complimentary low frequency Raman scattering for all materials in the same energy range as the QENS data (S8–S13), plots of the Boson Peak area (S14) and Lorentzian area (S15) as function of T–T_g and a statistical analysis of how

strongly KE_{50} correlates with the FWHM of the Lorentzian (S16). See DOI: https://doi.org/10.1039/d6sm00313c.

Acknowledgements

We acknowledge the support of the National Institute of Standards and Technology, U.S. Department of Commerce, in providing the neutron research facilities used in this work. The HFBS Spectrometer at the NIST Center for Neutron Research is supported in part by funding from the NSF as part of the Center for High Resolution Neutron Spectroscopy. The AGNES experiments were carried out through the JRR-3 general user program managed by the Institute for Solid State Physics, the University of Tokyo (Proposal No. 22406, 23406). Adam Burns, Katherine Evans, and Polette Centellas were supported by funding from the NIST-NRC Postdoctoral Research Fellowship program.

Notes and references

1 D. B. Knorr, J. H. Yu, A. D. Richardson, M. D. Hindenlang, I. M. McAninch, J. J. La Scala and J. L. Lenhart, Glass transition dependence of ultrahigh strain rate response in amine cured epoxy resins, *Polymer*, 2012, **53**(25), 5917–5923.

2 D. B. Knorr, K. A. Masser, R. M. Elder, T. W. Sirk, M. D. Hindenlang, J. H. Yu, A. D. Richardson, S. E. Boyd, W. A. Spurgeon and J. L. Lenhart, Overcoming the structural versus energy dissipation trade-off in highly crosslinked polymer networks: Ultrahigh strain rate response in polydicyclopentadiene, *Compos. Sci. Technol.*, 2015, **114**, 17–25.

3 E. D. Bain, D. B. Knorr, A. D. Richardson, K. A. Masser, J. Yu and J. L. Lenhart, Failure processes governing high-rate impact resistance of epoxy resins filled with core-shell rubber nanoparticles, *J. Mater. Sci.*, 2016, **51**(5), 2347–2370.

4 K. A. Masser, D. B. Knorr, J. H. Yu, M. D. Hindenlang and J. L. Lenhart, Dynamic heterogeneity in epoxy networks for protection applications, *J. Appl. Polym. Sci.*, 2016, **133**, 45.

5 T. R. Long, R. M. Elder, E. D. Bain, K. A. Masser, T. W. Sirk, J. H. Yu, D. B. Knorr and J. L. Lenhart, Influence of molecular weight between crosslinks on the mechanical properties of polymers formed via ring-opening metathesis, *Soft Matter*, 2018, **14**(17), 3344–3360.

6 K. A. Masser, T. R. Long, J. H. Yu, D. B. Knorr, M. D. Hindenlang, T. Taylor, D. Harris and J. L. Lenhart, The temperature-dependent ballistic performance and the ductile-to-brittle transition in polymer networks, *J Polym Sci Pol Phys*, 2019, **57**(9), 511–523.

7 R. M. Elder, D. B. Knorr, J. W. Andzelm, J. L. Lenhart and T. W. Sirk, Nanovoid formation and mechanics: a comparison of poly(dicyclopentadiene) and epoxy networks from molecular dynamics simulations, *Soft Matter*, 2016, **12**(19), 4418–4434, DOI: 10.1039/C6SM00691D.

8 R. M. Elder, T. R. Long, E. D. Bain, J. L. Lenhart and T. W. Sirk, Mechanics and nanovoid nucleation dynamics: effects of polar functionality in glassy polymer networks, *Soft Matter*, 2018, **14**(44), 8895–8911, DOI: 10.1039/C8SM01483C.

9 Y. Wada and T. Kasahara, Relation between Impact Strenght and Dynamic Mechanical Properties of Plastics, *J. Appl. Polym. Sci.*, 1967, **11**(9), 1661–1665.

10 G. Locati and A. V. Tobolsky, Studies of the toughness of polycarbonate of bisphenol a in light of its secondary transition, *Adv. Mol. Relax. Processes*, 1970, **1**(4), 375–408.

11 G. Allen, D. C. W. Morley and T. Willias, Impact Strength of Polycarbonate, *J. Mater. Sci.*, 1973, **8**(10), 1449–1452.

12 P. I. Vincent, Impact strength and mechanical losses in thermoplastics, *Polymer*, 1974, **15**(2), 111–116.

13 A. D. Mulliken and M. C. Boyce, Mechanics of the rate-dependent elastic–plastic deformation of glassy polymers from low to high strain rates, *Int. J. Solids Struct.*, 2006, **43**(5), 1331–1356.

14 S. Sarva and M. Boyce, Mechanics of polycarbonate during high-rate tension, *J. Mech. Mater. Struct.*, 2007, **2**(10), 1853–1880.

15 S. Sarva, A. D. Mulliken and M. C. Boyce, Mechanics of Taylor impact testing of polycarbonate, *Int. J. Solids Struct.*, 2007, **44**(7–8), 2381–2400.

16 C. L. Soles, A. B. Burns, K. Ito, E. Chan, J. W. Liu, A. F. Yee and M. S. Tyagi, Importance of Sub-Nanosecond Fluctuations on the Toughness of Polycarbonate Glasses, *Macromolecules*, 2020, **53**(15), 6672–6681.

17 C. L. Soles, A. B. Burns, K. Ito, E. P. Chan, J. F. Douglas, J. H. Wu, A. F. Yee, Y. T. Shih, L. P. Huang and R. M. Dimeo, *et al.*, Why Enhanced Subnanosecond Relaxations Are Important for Toughness in Polymer Glasses, *Macromolecules*, 2021, **54**(5), 2518–2528.

18 I. M. McAninch, G. R. Palmese, J. L. Lenhart and J. J. La Scala, Characterization of epoxies cured with bimodal blends of polyetheramines, *J. Appl. Polym. Sci.*, 2013, **130**(3), 1621–1631.

19 V. N. Novikov, Phonon-density fluctuations and fast relaxation in glasses, *Phys Rev B*, 1997, **55**(22), R14685–R14688.

20 T. Kanaya, T. Kawaguchi and K. Kaji, Local Dynamics of Some Bulk Polymers above Tg As Seen by Quasielastic Neutron Scattering, *Macromolecules*, 1999, **32**(5), 1672–1678.

21 R. M. Elder, A. L. Forster, A. Krishnamurthy, J. M. Dennis, H. Akiba, O. Yamamuro, K. Ito, K. M. Evans, C. Soles and T. W. Sirk, Relative effects of polymer composition and sample preparation on glass dynamics, *Soft Matter*, 2022, **18**(35), 6511–6516.

22 A. Meyer, R. M. Dimeo, P. M. Gehring and D. A. Neumann, The high-flux backscattering spectrometer at the NIST Center for Neutron Research, *Rev. Sci. Instrum.*, 2003, **74**(5), 2759–2777.

23 T. Kajitani, K. Shibata, S. Ikeda, M. Kohgi, H. Yoshizawa, K. Nemoto and K. Suzuki, Construction of the TOF-type cold-neutron spectrometer, AGNES, *Phys. B: Condens. Matter*, 1995, **213–214**, 872–874.

24 H. Akiba, Y. Ohmasa, M. Kofu, M. Zhang, S. Sato and O. Yamamuro, Improvement of a Time-of-Flight Spectrometer AGNES at JRR-3 Using Supermirror Techniques, *J. Phys. Soc. Jpn.*, 2024, **93**(9), 091010.

25 C. L. Soles, J. F. Douglas, W. L. Wu and R. M. Dimeo, Incoherent neutron scattering as a probe of the dynamics in molecularly thin polymer films, *Macromolecules*, 2003, **36**(2), 373–379.

26 C. L. Soles, J. F. Douglas, W. L. Wu and R. M. Dimeo, Incoherent neutron scattering and the dynamics of confined polycarbonate films, *Phys. Rev. Lett.*, 2002, **88**(3), 037401.

27 R. T. Azuah, L. R. Kneller, Y. M. Qiu, P. L. W. Tregenna-Piggott, C. M. Brown, J. R. D. Copley and R. M. Dimeo, DAVE: A Comprehensive Software Suite for the Reduction, Visualization, and Analysis of Low Energy Neutron Spectroscopic Data, *J. Res. Natl. Instrum. Stand.*, 2009, **114**(6), 341–358.

28 K. A. Bensley, R. V. Chimenti and S. E. Lofland, Low-Frequency Raman Spectroscopy of Polymers, *Macromol. Chem. Phys.*, 2025, **226**(15), 70004.

29 N. Shoji, K. Sasaki, A. Uedono, Y. Taniguchi, K. Hayashi, N. Matsubara, T. Kobayashi and T. Yamashita, Effect of conversion on epoxy resin properties: Combined molecular dynamics simulation and experimental study, *Polymer*, 2022, **254**, 125041.

30 K. Sasaki and T. Yamashita, Modification and Validation of the DREIDING Force Field for Molecular Liquid Simulations (DREIDING-UT), *J. Chem. Inf. Model.*, 2021, **61**(3), 1172–1179.

31 S. H. Chen, A. J. Souna, S. J. Stranick, M. Jhalaria, S. K. Kumar, C. L. Soles and E. D. P. Chan, Controlling toughness of polymer-grafted nanoparticle composites for impact mitigation, *Soft Matter*, 2022, **18**(2), 256–261.

32 B. Ruffle, D. A. Parshin, E. Courtens and R. Vacher, Boson peak and its relation to acoustic attenuation in glasses, *Phys. Rev. Lett.*, 2008, **100**(1), 015501.

33 V. L. Gurevich, D. A. Parshin and H. R. Schober, Anharmonicity, vibrational instability, and the Boson peak in glasses, *Phys Rev B*, 2003, **67**(9), 094203.

34 R. Zorn, Viewpoint: The boson peak demystified?, *Physics*, 2011, **4**, 44.

35 A. I. Chumakov, G. Monaco, A. Monaco, W. A. Crichton, A. Bosak, R. Rüffer, A. Meyer, F. Kargl, L. Comez and D. Fioretto, *et al.*, Equivalence of the Boson Peak in Glasses to the Transverse Acoustic van Hove Singularity in Crystals, *Phys. Rev. Lett.*, 2011, **106**(22), 225501.

36 H. Nakagawa, Y. Joti, A. Kitao and M. Kataoka, Hydration affects both harmonic and anharmonic nature of protein dynamics, *Biophys. J.*, 2008, **95**(6), 2916–2923.

37 F. Leonforte, A. Tanguy, J. Wittmer and J.-L. Barrat, Inhomogeneous elastic response of silica glass, *Phys. Rev. Lett.*, 2006, **97**(5), 055501.

38 S. Elliott, A unified model for the low-energy vibrational behaviour of amorphous solids, *Europhys. Lett.*, 1992, **19**(3), 201.

39 W. Schirmacher, Thermal conductivity of glassy materials and the ''boson peak, *Europhys. Lett.*, 2006, **73**(6), 892.

40 W. Schirmacher, G. Ruocco and T. Scopigno, Acoustic attenuation in glasses and its relation with the boson peak, *Phys. Rev. Lett.*, 2007, **98**(2), 025501.

41 Y.-C. Hu and H. Tanaka, Origin of the boson peak in amorphous solids, *Nat. Phys.*, 2022, **18**(6), 669–677.

42 C. Jiang, M. Baggioli and J. F. Douglas, Stringlet excitation model of the boson peak, *J. Chem. Phys.*, 2024, **160**(21), 214505.

43 C. L. Soles, R. M. Dimeo, D. A. Neumann, A. Kisliuk, A. P. Sokolov, J. W. Liu and A. F. Yee, Correlations of the boson peak with positron annihilation in series of polycarbonate copolymers, *Macromolecules*, 2001, **34**(12), 4082–4088.

44 A. P. Holt, D. Fragiadakis, J. A. Wollmershauser, B. N. Feigelson, M. Tyagi and C. M. Roland, Stability Limits of Pressure Densified Polycarbonate Glass, *Macromolecules*, 2019, **52**(11), 4139–4144.

45 L. Hong, B. Begen, A. Kisliuk, C. Alba-Simionesco, V. N. Novikov and A. P. Sokolov, Pressure and density dependence of the boson peak in polymers, *Phys Rev B*, 2008, **78**(13), 134201.

46 J. K. Gillham and S. L. Simon, Cure Property Diagrams for a Liquid Dicyanate Ester High-T(C) Polycyanurate Thermosetting System, *Abstr Pap Am Chem S*, 1994, **208**, 300–Pmse.

47 R. A. Venditti and J. K. Gillham, Anomalous Behavior of Thermosetting Systems after Cure Vs Chemical Conversion - a Normalized Conversion-Temperature-Property Diagram, *J. Appl. Polym. Sci.*, 1995, **56**(13), 1687–1705.

48 R. A. Venditti, J. K. Gillham, Y. C. Jean and Y. Lou, Free-Volume after Cure Vs Fractional Conversion for a High-T-G Epoxy-Amine Thermosetting System, *J. Appl. Polym. Sci.*, 1995, **56**(10), 1207–1220.

49 E. Donth, The size of cooperatively rearranging regions at the glass transition, *J. Non-Cryst. Solids*, 1982, **53**(3), 325–330.

50 C. Schick and E. Donth, Characteristic length of glass transition: experimental evidence, *Phys. Scr.*, 1991, **43**(4), 423.

51 G. Adam and J. H. Gibbs, On the Temperature Dependence of Cooperative Relaxation Properties in Glass-Forming Liquids, *J. Chem. Phys.*, 1965, **43**(1), 139–146.

52 L. M. Robeson, The effect of antiplasticization on secondary loss transitions and permeability of polymers, *Polym. Eng. Sci.*, 1969, **9**(4), 277–281.

53 L. M. Robeson and J. A. Faucher, Secondary loss transitions in antiplasticized polymers, *J. Polym. Sci., Part B: Polym. Lett.*, 1969, **7**(1), 35–40.

54 E. Sacher, The impact strength of polycarbonate, *J. Macromol. Sci., Part B*, 1974, **9**(1), 163–167.

55 M. G. Wyzgoski and G. S. Y. Yeh, Origin of impact strength in polycarbonate. III. Effect of liquids and orientation, *J. Macromol. Sci., Part B*, 1974, **10**(3), 441–476.

56 H. H. Kausch, *Intrinsic molecular mobility and toughness of polymers*, Springer, 2005.

57 S. Arrese-Igor, A. Arbe, A. Alegria, J. Colmenero and B. Frick, Short-time dynamics of phenylene-rings in bisphenol based engineering thermoplastics, *Chem. Phys.*, 2003, **292**(2), 363–370.

58 S. Arrese-Igor, A. Arbe, A. Alegría, J. Colmenero and B. Frick, Sub-Tg dynamics in polycarbonate by neutron scattering and its relation with secondary γ relaxation, *J. Chem. Phys.*, 2005, **123**(1), 014907.

59 S. Arrese-Igor, O. Mitxelena, A. Arbe, A. Alegría, J. Colmenero and B. Frick, Molecular motions in glassy polycarbonate below its glass transition temperature, *J. Non-Cryst. Solids*, 2006, **352**(42), 5072–5075.

60 S. Arrese-Igor, A. Arbe, A. Alegría, J. Colmenero and B. Frick, Phenylene ring dynamics in phenoxy and the effect of intramolecular linkages on the dynamics of some engineering

thermoplastics below the glass transition temperature, *Phys Rev E*, 2007, **75**(5), 051801.
61 S. Arrese-Igor, O. Mitxelena, A. Arbe, A. Alegría, J. Colmenero and B. Frick, Effect of stretching on the sub-${T}_{g}$ phenylene-ring dynamics of polycarbonate by neutron scattering, *Phys Rev E*, 2008, **78**(2), 021801.
62 S. Arrese-Igor, A. Arbe, B. Frick and J. Colmenero, Glassy Dynamics of Polystyrene by Quasielastic Neutron Scattering, *Macromolecules*, 2011, **44**(8), 3161–3168.
63 M. Jhalaria, Y. Cang, Y. C. Huang, B. Benicewicz, S. K. Kumar and G. Fytas, Unusual High-Frequency Mechanical Properties of Polymer-Grafted Nanoparticle Melts, *Phys. Rev. Lett.*, 2022, **128**(18), 187801.
64 D. Zeller, M. T. F. Telling, M. Zamponi, V. García Sakai and J. Peters, Analysis of elastic incoherent neutron scattering data beyond the Gaussian approximation, *J. Chem. Phys.*, 2018, **149**(23), 234908.
65 B. Frick and L. J. Fetters, Methyl Group Dynamics in Glassy Polyisoprene: A Neutron Backscattering Investigation, *Macromolecules*, 1994, **27**(4), 974–980.
66 M. Pramanik, E. W. Fowler and J. W. Rawlins, Another look at epoxy thermosets correlating structure with mechanical properties, *Polym. Eng. Sci.*, 2014, **54**(9), 1990–2004.
67 L. Hong, V. N. Novikov and A. P. Sokolov, Dynamic heterogeneities, boson peak, and activation volume in glass-forming liquids, *Phys Rev E*, 2011, **83**(6), 061508.
68 R. M. Elder, A. Zaccone and T. W. Sirk, Identifying Non-affine Softening Modes in Glassy Polymer Networks: A Pathway to Chemical Design, *ACS Macro Lett.*, 2019, **8**(9), 1160–1165.
69 B. H. Jones, F. M. C'deBaca, E. J. Nissen, A. Y. Ku, J. W. Kopatz, N. U. Huynh, S. C. Leguizamon and K. E. Van Meter, Static and Dynamic Thermomechanical Properties of Phase-Separated Epoxy Networks with Tuned Microstructures, *ACS Appl. Polym. Mater.*, 2024, **6**(21), 13147–13157.
70 M. Aoki, A. Shundo, R. Kuwahara, S. Yamamoto and K. Tanaka, Mesoscopic Heterogeneity in the Curing Process of an Epoxy–Amine System, *Macromolecules*, 2019, **52**(5), 2075–2082.
71 M. Aoki, A. Shundo, S. Yamamoto and K. Tanaka, Effect of a heterogeneous network on glass transition dynamics and solvent crack behavior of epoxy resins, *Soft Matter*, 2020, **16**(32), 7470–7478.
72 S. Yamamoto, R. Ida, M. Aoki, R. Kuwahara, A. Shundo and K. Tanaka, Formation Mechanism of a Heterogeneous Network in Epoxy Resins, *Macromolecules*, 2023, **56**(11), 3913–3921.
73 J. W. Woodcock, S. J. Stranick, A. P. Kotula, S. H. Chen, S. Engmann, J. W. Gilman and G. A. Holmes, Reaction-Induced structural and compositional heterogeneity in amine-cured epoxy/epoxy thermosets: Visualization of heterogeneity using fluorescence lifetime imaging microscopy (FLIM), *Polymer*, 2023, **273**, 125826.
74 H. K. Nguyen, A. Shundo, S. Yamamoto, K. Tanaka and K. Nakajima, Influence of network heterogeneity on the nanoscale mechanical properties of epoxy resins, *Polym. J.*, 2025, **57**(4), 367–375.
75 K. L. Ngai, L. R. Bao, A. F. Yee and C. L. Soles, Correlation of positron annihilation and other dynamic properties in small molecule glass-forming substances, *Phys. Rev. Lett.*, 2001, **87**(21), 215901.

